

Article

Degradation of Carbamazepine by Photo(electro)catalysis on Nanostructured TiO₂ Meshes: Transformation Products and Reaction Pathways

Silvia Franz ¹, Ermelinda Falletta ², Hamed Arab ¹, Sapia Murgolo ^{3,*}, Massimiliano Bestetti ¹ and Giuseppe Mascolo ^{3,*} 

¹ Department of Chemistry, Materials and Chemical Engineering “G.Natta”, Politecnico di Milano, 20133 Milano, Italy; silvia.franz@polimi.it (S.F.); arab.hamed@polimi.it (H.A.); massimiliano.bestetti@polimi.it (M.B.)

² Department of Chemistry, Università di Milano, 20133 Milano, Italy; ermelinda.falletta@unimi.it

³ Istituto di Ricerca sulle Acque, CNR, Via F. De Blasio 5, 70132 Bari, Italy

* Correspondence: sapia.murgolo@ba.irsa.cnr.it (S.M.); giuseppe.mascolo@ba.irsa.cnr.it (G.M.); Tel.: +39-0805820519 (S.M. & G.M.)

Received: 13 December 2019; Accepted: 22 January 2020; Published: 1 February 2020



Abstract: Carbamazepine (CBZ) is a pharmaceutical compound recalcitrant to conventional wastewater treatment plants and widely detected in wastewater bodies. In the present study, advanced oxidation processes for carbamazepine removal are investigated, with particular regard to the degradation pathways of carbamazepine by photoelectrocatalysis and conventional photocatalysis. Photoelectrocatalysis was carried out onto TiO₂ meshes obtained by Plasma Electrolytic Oxidation, a well-known technique in the field of industrial surface treatments, in view of an easy scale-up of the process. By photoelectrocatalysis, 99% of carbamazepine was removed in 55 min while only 65% removal was achieved by photolysis. The investigation of the transformation products (TPs) was carried out by means of UPLC-QTOF/MS/MS. Several new TPs were identified and accordingly reaction pathways were proposed. Above 80 min the transformation products disappear, probably forming organic acids of low-molecular weight as final degradation products. The results demonstrated that photoelectrocatalysis onto TiO₂ meshes obtained by plasma electrolytic oxidation is a useful alternative to common advanced oxidation processes as wastewater tertiary treatment aimed at removing compounds of emerging concern.

Keywords: immobilized catalyst; titanium dioxide; photoelectrocatalysis; heterogeneous photocatalysis; compounds of emerging concern; transformation products

1. Introduction

Organic micropollutants represent a group of contaminants of emerging concern (CECs) contained in the effluents of wastewater treatment plants. This class of substances includes pharmaceutical and personal care products, fire retardants, plasticizers, steroidal hormones, antibiotic resistance genes and many other groups of compounds [1,2]. Unfortunately, sometimes information about their toxicity are insufficient to define their maximal levels in drinking water. However, at the same time it has been estimated that every year about two million people die due to diseases related to unsafe water [3]. Because of the growth of the world population and the increase of water consumption in the agricultural and industrial sectors, water reuse represents an important challenge, in particular in regions suffering from water scarcity. The European Union started to consider the question of CECs

with the Directive 2013/39/EU, including new substance in the priority list of the Directive 2000/60/EC and fixing a watch list of 10 substances that need to be monitored to ensure water quality [4,5] (Decision 2015/495/EU and Decision 2018/840/EU).

The request to improve water quality and the difficulty to remove CECs by conventional treatments have driven the scientific community to focus its efforts in the development of alternative technologies in wastewater treatment plants (WWTPs).

In fact, the conventional strategies used to treat wastewater fail with CECs, leading to partial pollutant removal or degrading them into products that are still active [6–9]. In recent years, various removal process like adsorption, photochemical processes and biological treatments have been used for the removal of these harmful substances [10–15]. Advanced oxidation processes (AOPs) represent new and very promising technologies able to remove a wide range of micropollutants, due to the generation of highly reactive non-selective hydroxyl radicals. AOPs include photochemical, photocatalytic and chemical oxidation processes. Among the AOPs, the use of heterogenous photocatalysts has been proposed as an effective alternative for the degradation of various classes of compounds in water. In fact, heterogeneous photocatalysis is able to completely remove contaminants from the system and to reduce the formation of undesired byproducts, which may be even more toxic than the parent compound [16,17]. Although numerous semiconductor oxides could be used for environmental remediation purposes (TiO_2 , ZnO, MgO, WO_3 , etc.), TiO_2 is the most investigated photocatalyst because of its low cost, chemical and photochemical stability, well known high activity and abundance [18–22]. Free-suspending systems are inherently more efficient than the immobilized ones due to higher surface area [23,24]. However, they also suffer from severe disadvantages, such as catalyst loss and difficulty in recovery the catalyst at the end of the treatment, limiting their real application because of the poor quality of the treated effluent. The possibility to immobilize TiO_2 particles on large size supports allows us to overcome part of these inconveniences, facilitating the reuse of the catalyst in subsequent treatment cycles [25–27].

Titanium dioxide-based photoelectrocatalysis (PEC) is an interesting alternative to common AOPs for water treatment. Provided that good electrical contact could be established between the support and the catalyst and between the catalytic material, the electrical polarization of the catalyst prevents electron-hole recombination, potentially compensating the inherent lack of surface area.

TiO_2 photoactive coatings can be obtained by several techniques, such as sol-gel, chemical vapor deposition, radio frequency magnetron sputtering, plasma spray, electron beam evaporation, pulsed laser deposition, anodic oxidation and plasma electrolytic oxidation (PEO) [28–33]. Among them, electrochemical anodization allows the direct growth of the photoactive catalyst by oxidation of an electrically conducting support (e.g., a titanium mesh) providing good mechanical adhesion and electrical contact with the substrate [33–35]. Furthermore, the electrochemically generated films, though usually porous, grow in the form of continuous and homogeneous coatings thus showing an inherently higher electrical conductivity compared to particle-made supported films. In particular, the PEO process is known to be a consolidated technique in the field of industrial surface treatments, showing distinctive advantages compared to other traditional techniques such as chemical conversion or conventional anodizing [36]. Compared to traditional anodizing resulting in TiO_2 nanotube arrays, the PEO process works at higher currents and higher voltages. Processing times required to obtain crystalline films are of the order of only few minutes (less than 10 min) and the resulting films show a peculiar porous double-layered morphology [37]. Some of the authors recently reported that TiO_2 films obtained by PEO outperform TiO_2 nanotube arrays showing quantum yields higher than 90% in photon-to-electron conversion [32,38]. They also demonstrated that TiO_2 films obtained by PEO are effective in water decolourization by photoelectrocatalysis [39] and that the catalysts can be successfully reused several times and regenerated if necessary [40].

In the present study, we report our recent achievements in the reaction pathways of carbamazepine degradation by photoelectrocatalysis. For this purpose, carbamazepine was spiked in MilliQ water and the identification of the possible transformation products during photoelectrocatalysis was carried

out by linkage analysis. For comparison, reaction pathways during conventional photocatalysis using commercial TiO_2 powder (Degussa P25- TiO_2 nanoparticle) and during photolysis were also studied and discussed. The TiO_2 mesh employed in the photoelectrocatalytic reactions was obtained by PEO in view of a viable up-scaling and industrial application in water decontamination.

2. Results and Discussion

2.1. Characterization of the Nanostructured Catalyst

The characterization of the TiO_2 catalyst exploited in the present study was performed on sacrificial samples obtained in the same synthesis conditions used to prepare the TiO_2 meshes employed in the reactor. The TiO_2 catalyst showed a porous morphology typical of oxides obtained by PEO, where pores formed an interconnected sponge-like surface structure which became increasingly compact closer to the oxide/substrate interface (Figure 1a) [37]. Energy-dispersive X-ray spectroscopy (EDX) (Figure 1a, insert) confirmed that the TiO_2 catalyst contained only Ti and O. Image processing of the SEM surface micrographs provided surface porosity values of about 10%. Electrochemical Impedance Spectroscopy (EIS) was carried out to further investigate the structure of the oxide. The Bode plot shown in Figure A1 in the Appendix A shows two time-constants, confirming that the oxide consisted of a double-layered structure, namely a more porous surface layer and a more compact inner layer. The corresponding Nyquist plot in Figure 1b shows a normal distribution. In the insert in Figure 1b the equivalent circuit is sketched, where R_{el} accounts for the electrolyte and ohmic resistances, R_c and R_p represent the resistance of compact and porous layer, and the Q_c and Q_p represent the corresponding capacitance. According to the fitting of the electrochemical impedance spectra, the values of R_c and R_p were respectively $168 \pm 4.70 \text{ k}\Omega\cdot\text{cm}^2$ and $3.55 \pm 0.19 \text{ k}\Omega\cdot\text{cm}^2$, while Q_c and Q_p were respectively 31.7 ± 0.85 and 23.1 ± 0.79 . Therefore, most of the resistance of the TiO_2 coatings can be attributed to the compact layer, while the capacitance of the oxide is quite similar in the two layers.

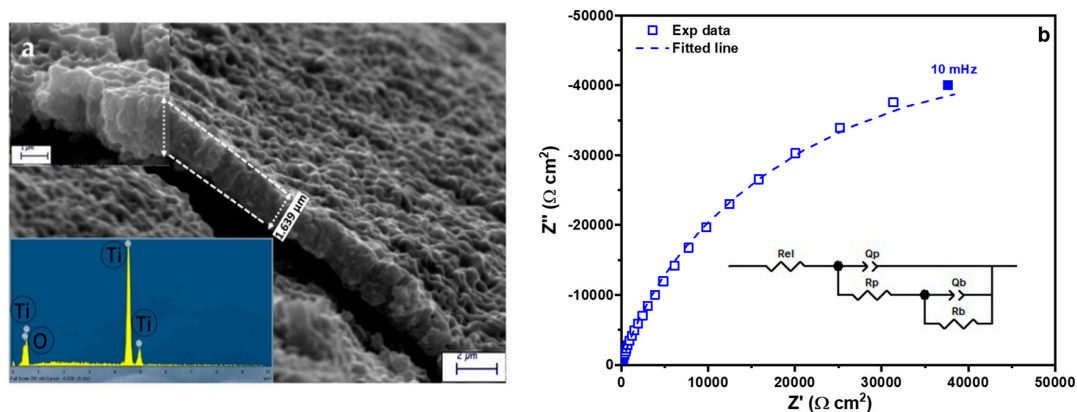


Figure 1. Cont.

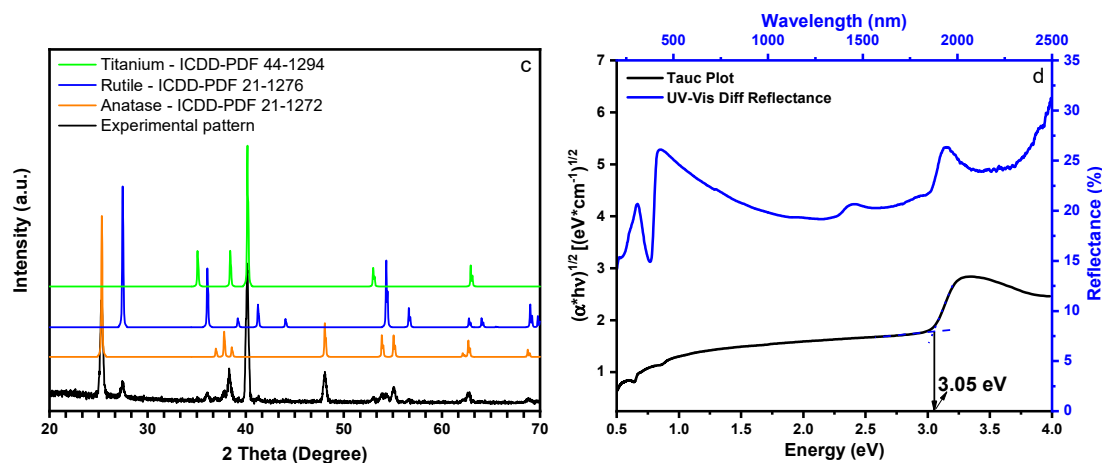


Figure 1. SEM micrographs, the left insets show a magnified SEM cross-section image and the EDX spectrum (a); Nyquist plot and fitting equivalent circuit (inset) (b); XRD pattern of the TiO₂ catalyst (experimental pattern) and the reference spectra for Anatase; Rutile; and Titanium (c); UV-VIS reflectance spectra (right and upper axes) and corresponding Tauc plot (left and lower axes) (d).

According to the GD-OES in-depth profiling shown in Figure A2 in the Appendix A, the thickness of the oxide film was about 2.5 μm , which is considered a reasonable compromise between high surface area and low probability of electron-hole recombination [41].

According to the XRD patterns in Figure 1c, the as-prepared oxide layers were crystalline in structure and consisted of a mixture of the anatase and rutile allotropic phases. The reflections at $2\theta = 25.31, 48.05, 53.89$ and 55.15 can be attributed to the anatase planes (101), (200), (105), (211) respectively. The rutile reflections appear at $2\theta = 27.48$ (110), 36.08 (101) and 54.31 (211). Reflections at $2\theta = 38.37$ and 40.18 can be attributed to the α -Titanium substrate. Based on Equation (2), the relative mass fraction of anatase and rutile phases was 58% and 42%, respectively. Based on UV-VIS spectroscopy and Kubelka-Munk conversion (Figure 1d), the energy band-gap was 3.06 eV, in agreement with the expectations considering the crystalline phase composition and the band-gap values of pure anatase and pure rutile, 3.2 eV and 3.02 eV, respectively [42–44].

The photoelectrochemical activity of the titanium dioxide coatings was assessed by current measurements under two electrical polarization conditions (open circuit and 0.6 V), both in the dark and under irradiation. During current measurements, the incident wavelength was linearly scanned from 310 nm to 430 nm in order to determine the optimal photoactivation wavelength. The photocurrent was calculated under the same polarization conditions as the difference between the current under irradiation minus the current in the dark. Finally, the Incident Photon-to Current Efficiency (IPCE), i.e., the capability of the oxide in converting the incident photons into photogenerated electrons, was calculated at each single irradiation wavelength using Equation (3). As shown in Figure 2, the IPCE of TiO₂ films represented as a function of the irradiation wavelength exhibited a non-symmetric bimodal distribution, with maximum values of 93% and 62% at 310 nm and 375 nm, respectively. The bimodal shape can be understood considering that the oxide consisted of a mixture of anatase and rutile phases, whose activation peaks are positioned at around 325 nm and 380 nm, respectively. The same Figure 2 also shows that the IPCE can be enhanced by applying a positive voltage of 0.6 V vs. SCE. Based on the abovementioned IPCE values, it was inferred that the TiO₂ catalyst under investigation could be well photoactivated by UV-C sources; it was also concluded that a slight anodic polarization would have further increased the photoactivity of the catalyst.

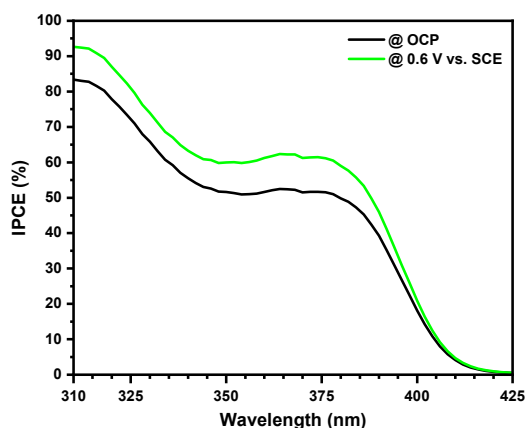


Figure 2. Incident photon to current efficiency (IPCE) of the TiO₂ catalyst as a function of incident light wavelength at open circuit and 0.6 V vs. saturated calomel electrode (SCE).

The minimum surface area of the TiO₂ catalyst was the geometrical area of the mesh, around 327.5 cm². To evaluate the surface enhancement due to porosity, ElectroChemical Surface Area (ECSA) measurements were carried out. The ECSA values were calculated on the basis of the capacitance of the layers by means of cyclic voltammetry at several scan rate and was performed in the non-faradaic region around the open-circuit potential value. The estimated ECSA was 5.7 m² g⁻¹ for the TiO₂ film, which seems to be a reasonable value when it is compared with real surface area of TiO₂ nano-powders as 50 m² g⁻¹. The surface area increase due to the porous structure of the TiO₂ film was 54.8 per unit geometrical area of mesh, corresponding to a total surface area of 1.795 m². Comparatively, given that the concentration of the TiO₂ nanopowders was 100 mg L⁻¹, the total surface area employed in conventional photocatalysis was 5 m². Considering that one of the main concerns using supported nanocatalyst is the reduction of surface area, in the present study due to surface morphology the supported catalyst showed a surface area which was of the same order of magnitude of the conventional TiO₂ Degussa P25.

2.2. Degradation of Carbamazepine

Figure 3 shows the degradation of carbamazepine under the investigated UV-assisted processes, namely: photoelectrocatalysis (UV + Bias + Mesh), photocatalysis using the TiO₂ mesh (UV + Mesh), electrochemical oxidation (Mesh + Bias), conventional photocatalysis (UV + Degussa P25) and photolysis (UV).

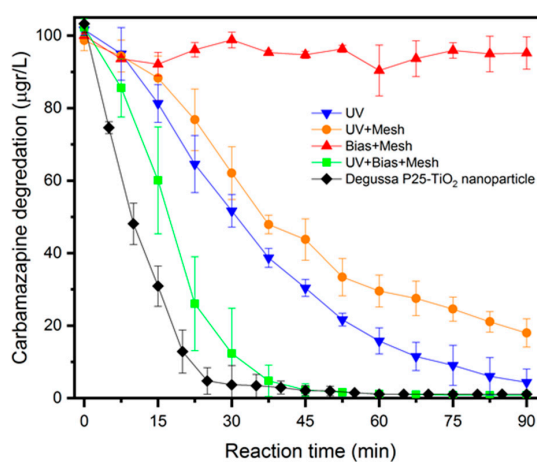


Figure 3. Degradation of carbamazepine by photoelectrocatalysis (UV + Bias + Mesh), photocatalysis on the TiO₂ mesh (UV + Mesh), electrochemical oxidation (Mesh + Bias), photolysis (UV) and conventional photocatalysis (UV + Degussa P25).

The results show that by photoelectrocatalysis a complete abatement of carbamazepine was obtained in 55 min. The beneficial effect given by the electrical polarization of the mesh is apparent when the UV + Mesh test is considered, where the catalyst was operating in open circuit conditions. The resulting degradation kinetics was significantly slower using the TiO₂ mesh in presence of the only UV source; after 55 min the residual concentration of carbamazepine was 35% and at the end of the test (90 min) it was about 17%. The photolysis process was carried in the same reactor after removing the TiO₂ mesh. As shown in Figure 3, the degradation was faster than in the UV + TiO₂ mesh process. A fast degradation kinetics was also observed by conventional photocatalysis with commercial TiO₂ powder (Degussa P25-TiO₂ nanoparticle), where a complete abatement of carbamazepine was obtained within 30 min.

However, to properly compare the three reactions, the results of the actinometric measurements should be taken into account. In fact, actinometry revealed that the TiO₂ mesh induced a shielding effect of the UV light, reducing the UV dosage on the water sample by 51% and the radiance density flux from 0.16 W cm⁻² to 0.08 W cm⁻². Similarly, it was assessed that the TiO₂ Degussa P25 powders produced a shielding effect of about 7%, the remaining radiance flux being 0.15 W cm⁻². As discussed in Section 2.1, based on ESCA measurements the total surface area of the TiO₂ mesh (about 1.8 m²) was of the same order of magnitude of the surface area of the TiO₂ nanopowders (5 m²). Therefore, the values of degradation rates of photolysis and conventional photocatalysis compared to (electro)catalytic counterparts (i.e., photocatalysis on supported TiO₂ and photoelectrocatalysis, respectively) can be mainly attributed to the different irradiation flux rather than to the different surface area. Despite the drawback consisting in the shielding effect of the mesh, the possibility of easily managing a supported catalyst, which does not need to be recovered with difficulty at the end of the treatment and it can be easily regenerated, makes electrochemical photocatalysis strongly advantageous if compared to conventional photocatalysis using commercial TiO₂ powder (Degussa P25-TiO₂ nanoparticle).

As shown in Figure A3 in the Appendix A, all results were well fitted by applying the Langmuir-Hinselwood model to a first order kinetics. From the value of the kinetic constants the Electrical Energy per Order of magnitude of removal (E_{EO}) of carbamazepine during investigated treatments was calculated according to Equation (1).

$$E_{EO} \text{ (kWhm}^{-3}\text{)} = \frac{38.4 \times UV \text{ power (kW)}}{V \text{ (l)} \times k \text{ (min}^{-1}\text{)}} \quad (1)$$

where k is the first-order rate constant in the different reaction configurations, V is the total volume of the treated water and $UV \text{ power}$ was obtained from the employed UV lamp.

The corresponding kinetic constants, half-life time and E_{EO} values are reported in Table 1.

Table 1. Kinetic constants, half-life times and Electrical Energy per Order of magnitude of removal (E_{EO}) of carbamazepine during degradation by photoelectrocatalysis (UV + Bias + Mesh), photocatalysis using the TiO₂ mesh (UV + Mesh), electrochemical oxidation using the TiO₂ mesh (Mesh + Bias), photolysis (UV) and photocatalysis using commercial TiO₂ powders (UV + Degussa P25).

Reactor Configuration	k (min ⁻¹)	h.l.t (min)	E_{EO} (KWh/m ³)
UV + Bias + Mesh	0.076 ± 0.002	17	7.58
UV + Mesh	0.018 ± 0.007	36	31.98
Mesh + Bias	0.0008 ± 0.0002	∞	719.55
UV	0.028 ± 0.001	31	20.55
UV + Degussa P25	0.174 ± 0.018 × 10 ⁻¹⁵	4.5	3.30

Based on the parameters reported in Table 1, it can be generally concluded that, excluding photoelectrocatalysis on TiO₂ powders which will be commented separately, the photoelectrocatalytic reaction was most efficient process. As for the kinetic constant, by applying a bias to the catalyst during operation (UV + Mesh + Bias) an increase by a factor of 4.2 was observed with respect to

photocatalysis on supported TiO₂ (UV + Mesh). The employment of a polarized catalyst increased the kinetic constant by a factor of 2.7 with respect to photolysis. Correspondingly, the half-life time changed. More interestingly, by applying an electrical polarization to the catalyst the E_{EO} decreased by a factor of 2.7 with respect to photolysis (i.e., from 20.55 kW/m³ to 7.58 kW/m³).

Photocatalysis using commercial TiO₂ powders was carried as it is considered a bench-mark to evaluate other AOPs. In this case, the fastest degradation kinetics was observed ($k = 0.174$). As previously mentioned, in the present study the ECSA of the supported TiO₂ catalyst (1.8 m²) and the surface area of the commercial TiO₂ powders (5 m²) were comparable. The different kinetics can be explained considering that the UV dosage using the mesh decreased by 51%, compared to 7% using the dispersed TiO₂ powders. However, this drawback is compensated by the mentioned technological advantage of using a supported catalyst, which does not need recovering of the catalyst after usage, can be used several times and can be easily regenerated in case of aging [40].

2.3. Identification of the Transformation Products and Degradation Pathways of Carbamazepine

The identification of possible transformation products (TPs) arising from uncompleted mineralization of carbamazepine was carried out by means of linkage analysis using LC-MS and LC-MS/MS investigation [45]. The analysis was done on the basis of both the accurate m/z ratio of all detected compounds and the corresponding fragmentation pattern, obtained by high resolution-mass spectrometry, along with elemental composition employing the isotopic distribution of molecular ion. Possible transformation products (TPs) were identified for all the investigated photodegradation processes, i.e., photoelectrocatalysis, photolysis and conventional photocatalysis, and listed in Tables 2–4, respectively. Based on the described approach for the identification of the TPs and according to Schymanski et al. [46], the identification level for detected TPs was 2 (probable structure), except for TP 129 formed during the photoelectrocatalysis treatment for which the identification level was 5 (exact mass of interest).

Table 2. Transformation products of carbamazepine by photoelectrocatalysis.

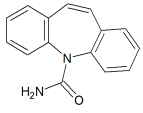
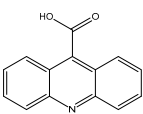
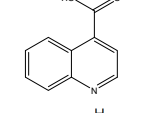
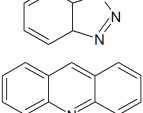
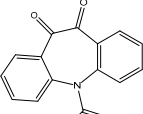
Product Code	m/z [M + H] ⁺	Elemental Composition	Structure	MS Error (ppm)	Trend	Refs
CBZ	237.1016	C ₁₅ H ₁₂ N ₂ O		5.0	descending	
TP129	130.9648	-	-	6.5	bell-shape	-
TP223	224.0695	C ₁₄ H ₉ NO ₂		7.4	bell-shape	[40,47]
TP173	174.0538	C ₁₀ H ₇ NO ₂		12.0	bell-shape	-
TP119	120.0547	C ₆ H ₅ N ₃		12.3	increasing	-
TP179	180.0794	C ₁₃ H ₉ N		10.7	bell-shape	[40,47–49]
TP266	267.0758	C ₁₅ H ₁₀ N ₂ O ₃		4.4	bell-shape	[40,48,50]

Table 2. Cont.

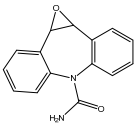
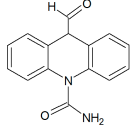
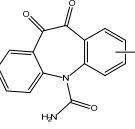
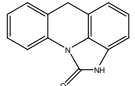
Product Code	m/z [M + H] ⁺	Elemental Composition	Structure	MS Error (ppm)	Trend	Refs
TP252-A	253.0966	C ₁₅ H ₁₂ N ₂ O ₂		4.4	bell-shape	[40,47–50]
TP252-B	253.0964	C ₁₅ H ₁₂ N ₂ O ₂		5.1	bell-shape	[51]
TP282	283.0708	C ₁₅ H ₁₀ N ₂ O ₄		3.8	bell-shape	[50]
TP222	223.086	C ₁₄ H ₁₀ N ₂ O		5.1	bell-shape	[51]

Table 3. Transformation products of carbamazepine (CBZ) by photolysis.

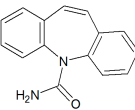
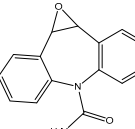
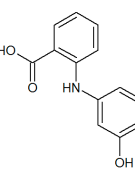
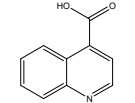
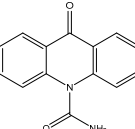
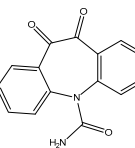
Product Code	m/z [M + H] ⁺	Elemental Composition	Structure	MS Error (ppm)	Trend	Refs
CBZ	237.1016	C ₁₅ H ₁₂ N ₂ O		5.0	descending	
TP252	253.0966	C ₁₅ H ₁₂ N ₂ O ₂		4.4	bell-shape	[40,47–50]
TP229	230.0807	C ₁₃ H ₁₁ NO ₃		4.4	increasing	-
TP173	174.0534	C ₁₀ H ₇ NO ₂		12.0	bell-shape	-
TP238	239.0805	C ₁₄ H ₁₀ N ₂ O ₂		6.5	bell-shape	-
TP266	267.0766	C ₁₅ H ₁₀ N ₂ O ₃		1.4	bell-shape	[40,48,50]

Table 3. Cont.

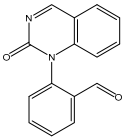
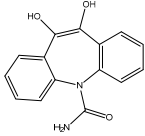
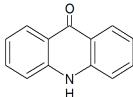
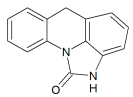
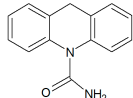
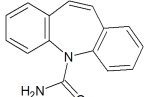
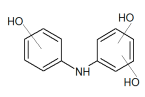
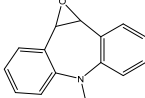
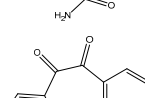
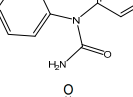
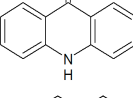
Product Code	m/z [M + H] ⁺	Elemental Composition	Structure	MS Error (ppm)	Trend	Refs
TP250	251.0804	C ₁₅ H ₁₀ N ₂ O ₂		6.6	bell-shape	[40,48]
TP268	269.0913	C ₁₅ H ₁₂ N ₂ O ₃		4.9	bell-shape	[48]
TP195	196.0744	C ₁₃ H ₉ NO		9.4	bell-shape	[47,48,50]
TP222	223.0857	C ₁₄ H ₁₀ N ₂ O		5.1	bell-shape	[51]
TP224	225.1022	C ₁₄ H ₁₂ N ₂ O		2.6	bell-shape	-

Table 4. Transformation products of carbamazepine by photocatalysis employing conventional commercial TiO₂ powder (Degussa P25-TiO₂ nanoparticle).

Product Code	m/z [M + H] ⁺	Elemental Composition	Structure	MS Error (ppm)	Trend	Refs
CBZ	237.1017	C ₁₅ H ₁₂ N ₂ O		4.6	descending	-
TP217	218.0816	C ₁₂ H ₁₁ NO ₃		0.5	increasing	-
TP252	253.0965	C ₁₅ H ₁₂ N ₂ O ₂		4.8	bell-shape	[40,47–50]
TP266	267.0766	C ₁₅ H ₁₀ N ₂ O ₃		1.4	bell-shape	[40,48,50]
TP195	196.075	C ₁₃ H ₉ NO		6.3	bell-shape	[47,48,50]
TP250	251.0804	C ₁₅ H ₁₀ N ₂ O ₂		6.6	bell-shape	[40,48]

The results show that several intermediates were produced during all the investigated processes. Although many of these are already known in the literature, several new transformation products

were identified. Ten TPs were identified during photoelectrocatalysis, three of them (TP119, TP129 and TP173) being new carbamazepine TPs. The same number of transformation products were identified during photolysis, out of them four being new TPs (TP173, TP224, TP229 and TP238). By conventional photocatalysis, only five transformation products were determined, and out of them TP217 is not reported in literature. Carbamazepine exhibits a constant decreasing profile in all the tested processes. The detected TPs showed two different types of time profiles, i.e., a bell-shape trend and a constant increase during the reaction time.

The time-profiles of all identified TPs, obtained by plotting the peak area of each selected TP along reaction time, are shown in Figure A4 in the Appendix A.

Most part of these TPs show a bell shape trend. Only a few TPs show an increasing concentration, corresponding to TPs accumulation in the reaction mixture. This is an evidence that UV-based processes represent a good alternative to traditional degradation approaches, reducing by-products accumulation in the treated wastewater. In particular, the time-profile plots revealed that the photoelectrocatalytic reaction generates TPs with higher intensity respect to photolysis with a subsequently faster abatement for all of them, except for TP120 for which a slight peak area increase along time of treatment was observed without no further degradation. Compared to conventional photocatalysis, despite the larger number of TPs the overall abatement by photoelectrocatalysis was obtained in shorter reaction times. This is also evident considering the two TPs (TP252 and TP266) occurring in all the three reactions (Figure 4), where the shortest degradation times were observed by photoelectrocatalysis. The results confirm that photoelectrocatalysis can outperform photolysis and compare to conventional photocatalysis. It must also be mentioned that only for photoelectrocatalysis smaller compounds were found, such as TP119 and TP173, confirming the higher degradation abilities of this approach if compared to the others. In both photoelectrocatalysis and conventional photocatalysis with Degussa (P25) at reaction times higher than 80 min the TPs disappear, probably producing small organic acids whose low-molecular weight (e.g., formic acid, acetic acid, etc. [52]) requires the use of a different analytical technique, such as ion chromatography, for detection and identification [53].

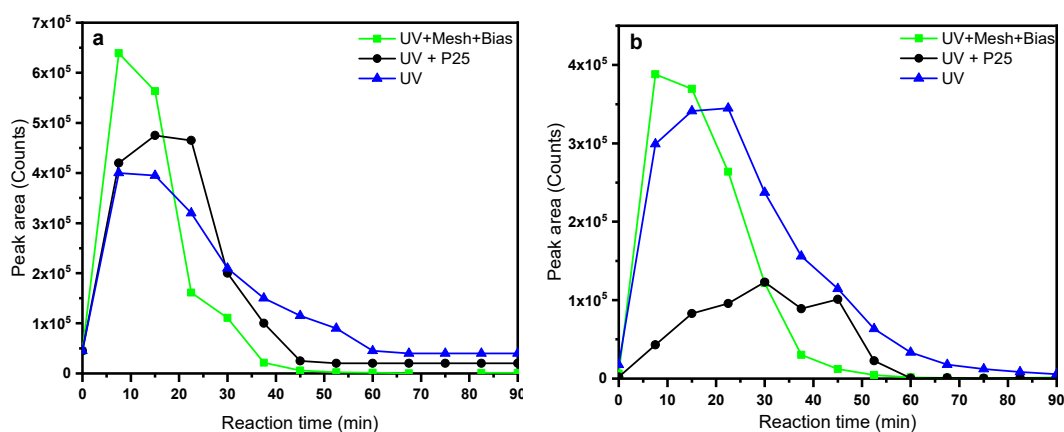


Figure 4. Time-resolved profiles of TP252 (a) and TP266 (b) of carbamazepine obtained by all the investigated processes.

Based on the identified TPs, a reaction pathway was proposed for photoelectrocatalysis (Figure 5), photolysis (Figure 6) and conventional photocatalysis (Figure 7). The pathways shown in Figures 5–7, mostly consist in oxidation reactions resulting in multiple-step degradation mechanism.

As for the photoelectrocatalytic treatment two possible reaction pathways were proposed: (i) an increase of 16 Da from CBZ was indicative of an oxidation reaction forming the TP252-A; from this transformation product a contraction of the 7-membered ring into a 6-membered ring within a loss of -CHNO group was proposed to produce TP223. Both TP 179 (acridine) and TP 173 were rationalized to derive from TP223 as results of multiple transformations. Sequential oxidation reactions transformed the intermediary TP252-A in TP266 and subsequently in TP282 by means of a hydroxylation reaction

based on an increase of 16 Da [50]; (ii) an hydroxylation and ring contraction of CBZ produced TP252-B subsequently transformed in TP222 through an intramolecular ring formation and loss of the aldehyde group. One more compound of MW 120.0547 ($[M + H]^+$) was identified, TP119, and based on both the predicted elemental composition and MS/MS fragmentation spectra a molecular structure was proposed (Table 2).

According to the reaction pathway supposed for the photolytic process, an increase of 16 Da was also in this case indicative of CBZ oxidation in TP252 and from this product two possible reactions were suggested: (i) consecutive oxidation reactions transforming the intermediary TP252 in TP268 and subsequently in TP266 from which TP 250 was rationalized to derive by a hydration reaction [40]; (ii) a contraction of the 7-membered ring into a 6-membered ring to produce the TP238 from which a loss of $-CHNO$ group was indicative for the production of TP195, with a decrease of 43 Da in terms of m/z , whereas the loss of the ketonic group and the subsequent cyclization resulted in TP224 and TP222, respectively. Two more compounds of MW 230.0808 and 174.0534 ($[M + H]^+$) were identified, TP229 and TP173 respectively, and based on both the predicted elemental composition and MS/MS fragmentation spectra a molecular structure was proposed (Table 3).

Finally, the detected TPs produced during the carbamazepine degradation by conventional photocatalysis with TiO_2 Degussa P25 revealed two possible reactions: (i) consecutive CBZ oxidation in TP252 and then TP266 subsequently transformed in TP250 by a hydration reaction; a contraction of the seven-membered ring into a six-membered ring to form the TP195 as result of multiple intermediate transformations. One more compound of MW 218.0816 ($[M + H]^+$) was identified, TP217, and based on both the predicted formula and MS/MS fragmentation a molecular structure was proposed (Table 4).

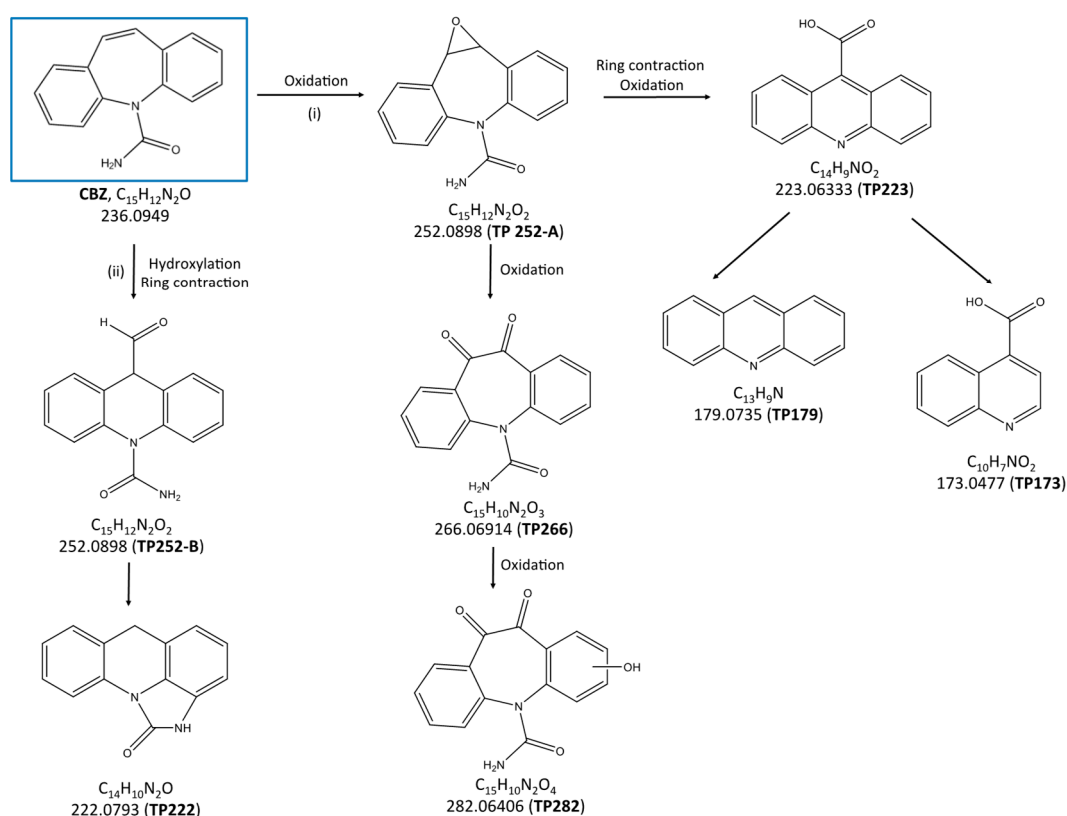


Figure 5. Proposed degradation pathway of carbamazepine degradation by photoelectrocatalysis obtained on the basis of the identified transformation products (TPs).

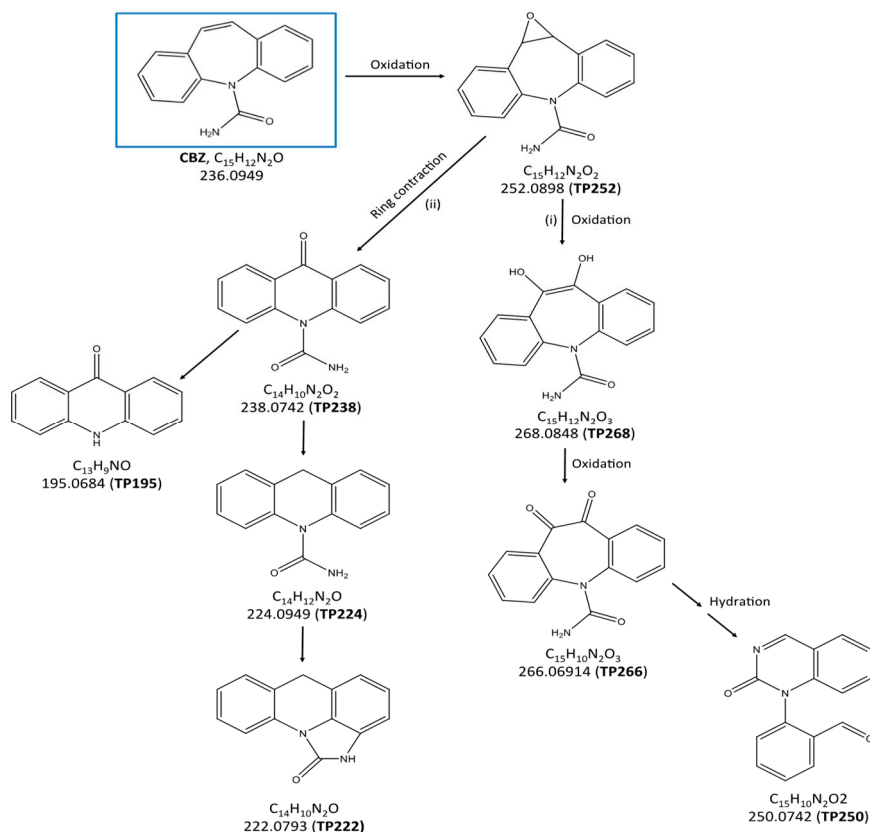


Figure 6. Proposed degradation pathway of carbamazepine degradation by photolysis obtained on the basis of the identified TPs.

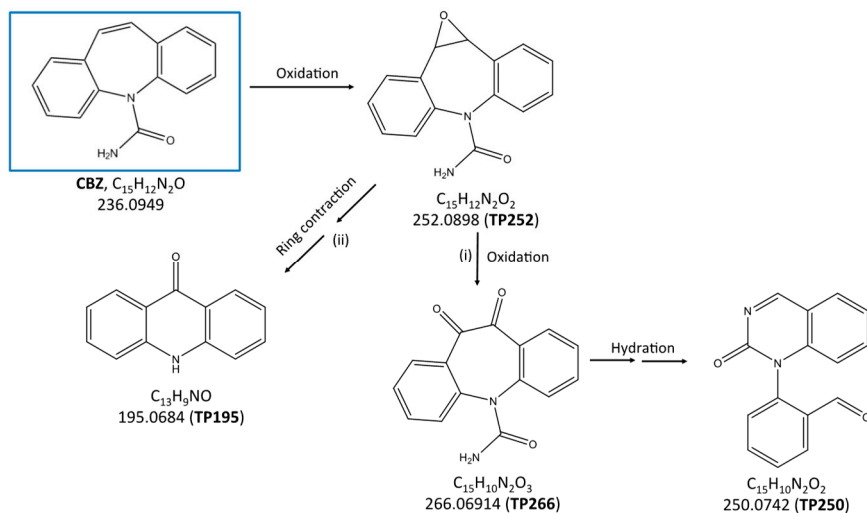


Figure 7. Proposed degradation pathway of carbamazepine degradation by conventional photocatalysis obtained on the basis of the identified TPs.

3. Materials and Methods

3.1. Synthesis and Characterization of the Nanostructured TiO_2 Catalyst

The titanium dioxide catalyst was prepared by Plasma Electrolytic Oxidation in 1.5 M H_2SO_4 (14.7 wt.%) solutions prepared with distilled water for 5 min at constant potential of 150 V. Grade 1 Titanium expanded meshes having geometric surface area 327.5 cm^2 were used as anodes. During the PEO synthesis, the electrolyte temperature was refrigerated at about $-5\text{ }^\circ\text{C}$ by means of a cryostat

(HAAK D10). After PEO, the expanded meshes were rinsed with water and dried in a stream of air. For further characterization, several smaller samples having an area of 18 cm² were also prepared. Under visual observation, the TiO₂ catalyst appeared uniform and light gray coloured. Morphology was observed by scanning electron microscopy (SEM) using a Zeiss EVO 50 instrument. The phase structure and texture of the titanium dioxide films were determined by X-ray diffraction (XRD) using a Philips PW1830 instrument. Diffractograms were acquired in Bragg-Brentano geometry at a potential of 40 kV with a filament current of 40 mA. The CuKα1 radiation was exploited at the scanning rate of 2.5° per min in the 2θ range 20–60°. The powder diffraction files of titanium (ICDD-PDF 44-1294), anatase (ICDD-PDF 21-1272) and rutile phases (ICDD-PDF 21-1276) were used to index the XRD patterns. The mass fraction of anatase was calculated by Equation (2) following Spurr and Meyer [54], where I_R is the intensity of the strongest rutile reflection, (110), and I_A is the intensity of the strongest anatase reflection, (101),

$$f_A = \frac{1}{\left(1 + 1.26 \frac{I_R}{I_A}\right)} \% \quad (2)$$

Surface porosity was evaluated by ImageJ, an open-source tool for the processing of scientific images. A number of SEM surface micrographs acquired at 20,000× were used for this purpose. Glow Discharge Optical Emission Spectrometry (GD-OES) was exploited to determine film thickness and depth profiling. GDOES analysis was carried on sample areas of ~2.5 mm diameter by means of a analyzer (Spectrumba GDA750) operating at 700 V in Ar atmosphere at 230 Pa. The monitored light emission wavelength was 130 nm and 362 nm for O and Ti, respectively.

The estimation of the electrochemical surface area (ECSA) of the TiO₂ obtained by PEO was done by performing cyclic voltammetry [55], where consecutive potential cycles centered around the open circuit potential were recorded in a potential window of 100 mV vs. SCE at five different scan rate.

The photoelectrochemical activity of the TiO₂ film was measured using a three electrode PEC cell with separated anodic and cathodic compartments. A TiO₂ electrode was used as working electrode, a platinum foil (25 × 25 mm²) as counter electrode and a saturated calomel electrode (SCE) as reference electrode. The photocurrent and corresponding incident photon to current efficiency (IPCE) were determined using an optical bench where the light source was a 300 W Xe lamp (Lot-qd), the monochromator was a LOT-qd Omni-λ 150 instrument, the shutter was Thorlabs SC10 tool, and the electrochemical cell was a homemade Plexiglas reactor presenting with an Pyrex optical glass window. The photocurrent measurements were carried out in a 1.0 M NaOH solution without and with applying an external bias (0.6 V vs. SCE) using an Amel mod. 2549 potentiostat/galvanostat and a digital multimeter (Tektronix DMM4040). The incident wavelength values ranged from 250 nm to 450 nm with a step of 2 nm and a dwell time of 4 s per step. A calibrated Thorlabs S130VC photodiode connected to a Thorlabs PM200 power meter was applied to measure the incident light power. To account for the transmittance of the cell window, a Pyrex window was placed in between. The IPCE percentage at each wavelength was calculated using the following Equation (3):

$$IPCE (\%) = \frac{h \times c}{e} \times \frac{I}{P \times \lambda} \quad (3)$$

where h is the Plank constant [m² Kg/s], c is the speed of light [m/s], e is the electron charge [C], I is the steady-state photocurrent density [A/m²], P is the light intensity [W/m²] and λ is the incident wavelength.

3.2. Bench-Scale Experiments

Degradation tests were carried out on 100 µg L⁻¹ (100 ppb) Carbamazepine (Sigma-Aldrich, Germany) dissolved in MilliQ water. The chemical structure of carbamazepine is displayed in Figure 8. The carbamazepine concentration was chosen as good compromise between having a concentration

high enough to allow the detection of several transformation products and low enough to simulate real environmental conditions [56,57].

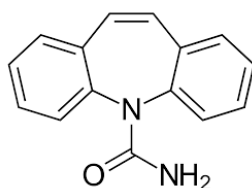


Figure 8. The structure of Carbamazepine.

The experiments were carried out in a laboratory-scale tubular stainless steel reactor having a volume of 1 L which is schematically represented in Figure 9. The reactor was equipped with a 2 L buffer reservoir and worked in semi-batch mode. An Iwaky Magnet Pump MD-30RZ-220N with a nominal power of 80 W was used to recirculate the carbamazepine solution. The water sample was pumped through the reactor up-flow. The UV lamp was a 30 W low-pressure Hg vapor lamp UV-C lamp emitting at 254 nm. A tubular expanded titanium mesh (geometric surface area 327.5 cm²) coaxially surrounded the UV lamp at a constant distance of a few mm. During the PEC experiments, an anodic bias of 4 V was applied to the anodized titanium mesh and a cathodic bias to the steel reactor body by means of an AMEL 2549 potentiostat/galvanostat. Actinometry test was exploited using 10 mM uridine (Sigma-Aldrich, Germany) considering the radiance density flux at 254 nm to quantify the shading effect of TiO₂ mesh on the UV dosage.

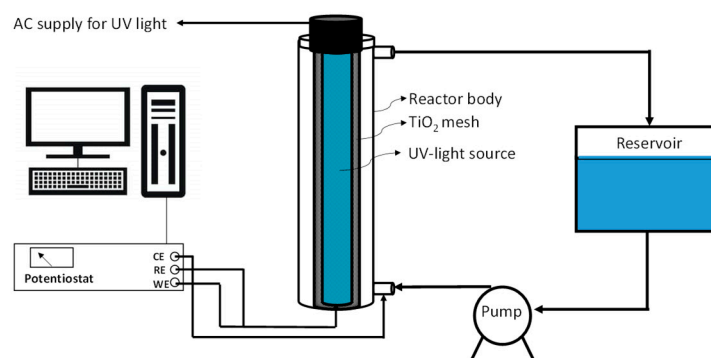


Figure 9. Schematic of the laboratory-scale electrochemical photoreactor working in up-flow condition and semi-batch mode.

Exploiting the described reactor, four different configurations were tested: UV + Bias + Mesh, UV + Mesh, Mesh + Bias, and UV. Test using a commercial TiO₂ powder (Degussa P25-TiO₂ nanoparticle) and named UV + Degussa P25, was performed using a tubular reactor (1 L) equipped with a 30 W low-pressure Hg vapor lamp (Helios Italquartz) and working in batch mode. The employed catalyst was Degussa P25 (Evonik) TiO₂, having an anatase-to-rutile ratio of typically of 80:20, an average diameter of 30 nm and a surface area of 50 m² g⁻¹. Each test was repeated three times.

3.3. Analytical Set-Up and Data Processing

The analytical set-up used both to monitor the residual concentration of carbamazepine and to identify TPs consisted of a TripleTOF 5600+ high-resolution mass spectrometer (AB-Sciex) interfaced with an Ultimate 3000 UPLC System (Thermo Fisher Scientific, Waltham, MA, USA). The mass spectrometer was equipped with a duo-spray ion source operating in positive and negative electrospray (ESI) mode. The MS analysis was accomplished following an information-dependent acquisition (IDA) method, including a full scan acquisition in TOF-MS, a background subtraction and the subsequent isolation and fragmentation in the collision cell of the 4 most intense ions. The chromatographic

separation of the analytes was carried out using an Acquity BEH C18 column, 2.1×150 mm, $1.7 \mu\text{m}$, operating at $0.200 \text{ mL min}^{-1}$.

500 μL samples were injected by a large volume injection mode in order to reach detection limit of the order of few ng L^{-1} and eluted with a binary gradient consisting of $\text{H}_2\text{O}/\text{ACN}$ 95/5 (A) and ACN (B) both with 0.1% HCOOH as follows: 5% B held for 4.6 min, linearly increased to 80% of B in 18.5 min and to 100% of B in further 5.5 min and kept for 5 min. The final eluent composition was then brought to 5% of B in 0.5 min and left to equilibrate the system for 10 min before the next run of analysis.

The residual concentration of CBZ was quantified by MultiQuant software (AB Sciex).

As for data processing, identification of both already known in literature and new TPs was performed by a suspect target and non-target screening employing data acquired with high resolution mass spectrometry (HRMS). All the analyzed samples, collected during each investigated treatment at different reaction times were processed using a detailed analytical protocol, including the following steps:

- i. the AB-Sciex software namely SciexOS, PeakView and MasterView were employed to screen samples for a list of known TPs (collected from data reported in the literature or from prediction models) based on the mass exact, isotopic cluster, fragmentation MS/MS spectrum and estimated chromatographic retention time (suspect target screening);
- ii. for each acquired file, a list of precursor ions with a specific retention time and peak intensity was generated by an open source software (i.e., *enviMass*); the list of detected ions was successively reduced by replicate sample intersection, isotope grouping and adduct grouping. Moreover, the list of detected ions was reduced by removing ions which have also been detected in blank samples (non-target screening);
- iii. the reduced peak list was processed by SciexOS software using both the formula finder algorithm (which tries to predict the possible chemical formula based on the MS and MS/MS spectrum using the precursor ion's mass accuracy, isotopic pattern and MS/MS fragmentation pattern) and the library searching capabilities (*LibraryView*). Structure identification was carried out based on high resolution MS/MS data [17]. For a more confident identification, the detected compound were linked to ChemSpider and Metlin [58].
- iv. Finally, in order to obtain additional information about the occurrence of possible TPs the final peak list was processed using a linkage analysis script in R statistical environment [47].

4. Conclusions

The application of a novel TiO_2 supported catalyst obtained by Plasma Electrolytic Oxidation employed in photoelectrocatalytic processes was investigated for the removal of a well-known recalcitrant emerging contaminant, i.e., carbamazepine, as a useful alternative to common advanced oxidation processes (AOPs). For comparison, the performance of both conventional photocatalysis using commercial TiO_2 powder (Degussa P25- TiO_2 nanoparticle) and photolysis were also studied and discussed.

Results showed that with Titanium dioxide-based photoelectrocatalysis a complete abatement of carbamazepine was obtained in 55 min under the investigated conditions. The resulting degradation kinetics was significantly slower using the TiO_2 mesh in presence of the only UV source and with respect to the photolysis, although instead conventional photocatalysis showed a higher degradation efficiency in carbamazepine removal.

However, the possibility of easily managing a supported catalyst, which does not need to be recovered with difficulty at the end of the treatment and easily prepared by a well-established technique in the field of industrial surface treatments makes electrochemical photocatalysis strongly advantageous if compared to conventional commercial TiO_2 powder (Degussa P25- TiO_2 nanoparticle). Moreover, the identification of the possible transformation products formed during the investigated treatments revealed that compared to conventional photocatalysis, despite the larger number of TPs, the overall abatement by photoelectrocatalysis was obtained in shorter reaction times.

It follows that the investigated treatment is a suitable oxidation process for practical applications in the field of water treatment as wastewater tertiary treatment aimed at removing compounds of emerging concern.

Author Contributions: S.F. carried out original draft writing, reviewing and editing, supervised the synthesis of the TiO_2 catalyst and the degradation experiments; H.A. synthesized the TiO_2 catalyst, performed the degradation experiments and contributed to the original draft writing; E.F. carried out data analysis, in particular for the identified the transformation products and contributed to original draft writing; S.M. carried out sample analysis, data collection and analysis; M.B. provided the resources needed for the synthesis of the catalyst and the degradation experiments; S.M. and G.M. supervised the overall activity, with particular regard to sample analysis and identification of transformation products, they also carried out draft reviewing. All authors have read and agreed to the published version of the manuscript.

Funding: This research received no external funding.

Acknowledgments: Elena Selli and Gian Luca Chiarello (University of Milano) for the IPCE measurements, Antonello Vicenzo and Maksim Bahdanchyk (Politecnico of Milano) for discussion on electrochemical impedance spectroscopy.

Conflicts of Interest: The authors declare no conflict of interest.

Appendix A

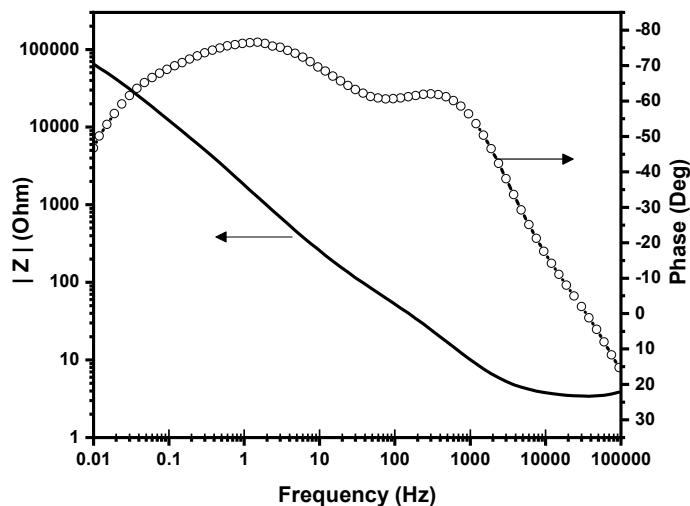


Figure A1. Bode plot performed at OCP and in $\text{NaOH}(1\text{M})$.

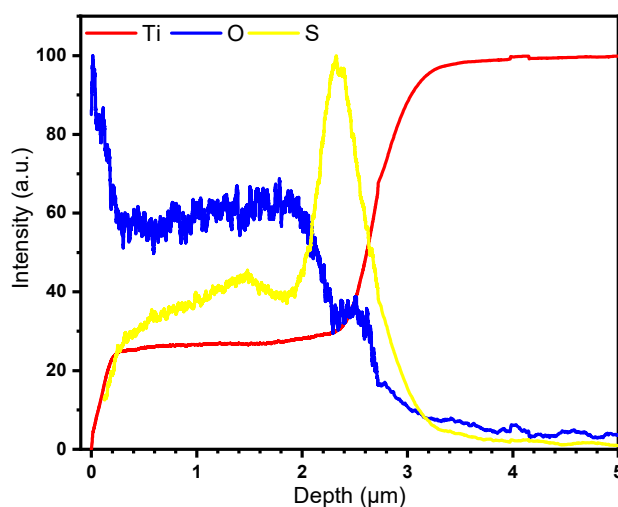


Figure A2. GD-OES in depth profile of TiO_2 film.

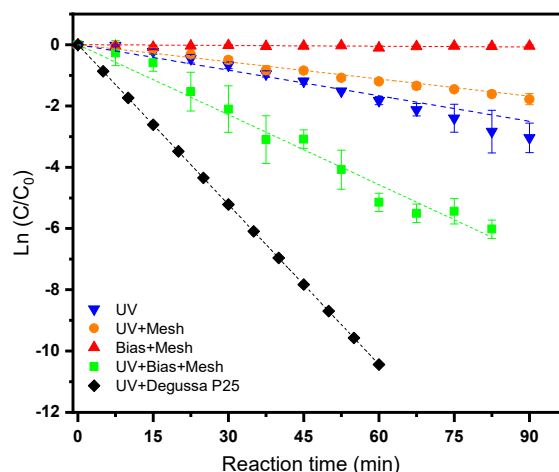


Figure A3. Fitted data by applying the Langmuir-Hinshelwood model reduced to a first order kinetics.

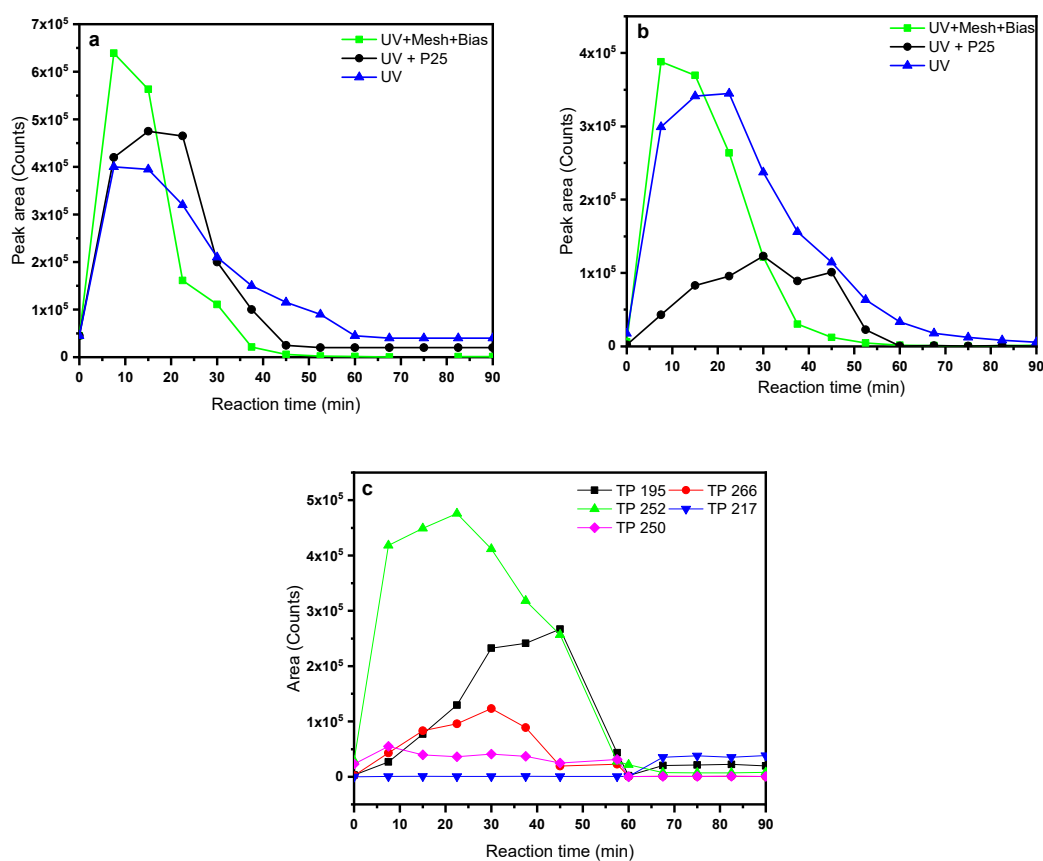


Figure A4. Time-profiles of the all the TPs at different reactor configuration: (a) Photo-electrocatalysis, (b) Photolysis, and (c) conventional photocatalysis with TiO₂ Degussa P25.

References

1. Sopilniak, A.; Elkayam, R.; Rossin, A.V.; Lev, O. Emerging organic pollutants in the vadose zone of a soil aquifer treatment system: Pore water extraction using positive displacement. *Chemosphere* **2018**, *190*, 383–392. [[CrossRef](#)] [[PubMed](#)]
2. Jiménez-Tototzintle, M.; Ferreira, I.J.; da Silva Duque, S.; Guimarães Barrocas, P.R.; Saggiaro, E.M. Removal of contaminants of emerging concern (CECs) and antibiotic resistant bacteria in urban wastewater using UVA/TiO₂/H₂O₂ photocatalysis. *Chemosphere* **2018**, *210*, 449–457. [[CrossRef](#)] [[PubMed](#)]
3. Suhogusoff, A.V.; Hirata, R.; Ferrari, L.C.K.M. Water quality and risk assessment of dug wells: A case study for a poor community in the city of São Paulo, Brazil. *Environ. Earth Sci.* **2013**, *68*, 899–910. [[CrossRef](#)]

4. The European Commission. Commission Implementing Decision (EU) 2015/495 of 20 March 2015 establishing a watch list of substances for Union-wide monitoring in the field of water policy pursuant to Directive 2008/105/EC of the European Parliament and of the Council. *Off. J. Eur. Union* **2015**, *78*, 40–42.
5. The European Commission. Commission Implementing Decision (EU) 2018/840 of 5 June 2018 establishing a watch list of substances for Union-wide monitoring in the field of water policy pursuant to Directive 2008/105/EC of the European Parliament and of the Council and repealing Commission Implementing Decision (EU) 2015/495. *Off. J. Eur. Union* **2018**, *141*, 9–12.
6. Zwiener, C.; Seeger, S.; Glauner, T.; Frimmel, F. Metabolites from the biodegradation of pharmaceutical residues of ibuprofen in biofilm reactors and batch experiments. *Anal. Bioanal. Chem.* **2002**, *372*, 569–575. [[CrossRef](#)]
7. Kümmerer, K.; Steger-Hartmann, T.; Meyer, M. Biodegradability of the anti-tumour agent ifosfamide and its occurrence in hospital effluents and communal sewage. *Water Res.* **1997**, *31*, 2705–2710. [[CrossRef](#)]
8. Ternes, T.A. Occurrence of drugs in German sewage treatment plants and rivers. *Water Res.* **1998**, *32*, 3245–3260. [[CrossRef](#)]
9. Balest, L.; Mascolo, G.; Di Iaconi, C.; Lopez, A. Removal of endocrine disrupter compounds from municipal wastewater by an innovative biological technology. *Water Sci. Technol.* **2008**, *58*, 953–956. [[CrossRef](#)]
10. Baghdadi, M.; Ghaffari, E.; Aminzadeh, B. Removal of carbamazepine from municipal wastewater effluent using optimally synthesized magnetic activated carbon: Adsorption and sedimentation kinetic studies. *J. Environ. Chem. Eng.* **2016**, *4*, 3309–3321. [[CrossRef](#)]
11. De Laurentiis, E.; Chiron, S.; Kouras-Hadef, S.; Richard, C.; Minella, M.; Maurino, V.; Minero, C.; Vione, D. Photochemical fate of carbamazepine in surface freshwaters: Laboratory measures and modeling. *Environ. Sci. Technol.* **2012**, *46*, 8164–8173. [[CrossRef](#)] [[PubMed](#)]
12. Kosjek, T.; Andersen, H.R.; Kompare, B.; Ledin, A.; Heath, E. Fate of carbamazepine during water treatment. *Environ. Sci. Technol.* **2009**, *43*, 6256–6261. [[CrossRef](#)] [[PubMed](#)]
13. Haroune, L.; Salaun, M.; Ménard, A.; Legault, C.Y.; Bellenger, J.-P. Photocatalytic degradation of carbamazepine and three derivatives using TiO₂ and ZnO: Effect of pH, ionic strength, and natural organic matter. *Sci. Total Environ.* **2014**, *475*, 16–22. [[CrossRef](#)] [[PubMed](#)]
14. Lopez, A.; Mascolo, G.; Tiravanti, G.; Passino, R. Degradation of herbicides (ametryn and isoproturon) during water disinfection by means of two oxidants (hypochlorine and chlorine dioxide). *Water Sci. Technol.* **1997**, *35*, 129–136. [[CrossRef](#)]
15. Raja, P.; Bozzi, A.; Jardim, W.F.; Mascolo, G.; Renganathan, R.; Kiwi, J. Reductive/oxidative treatment with superior performance relative to oxidative treatment during the degradation of 4-chlorophenol. *Appl. Catal. B Environ.* **2005**, *59*, 249–257. [[CrossRef](#)]
16. Rimoldi, L.; Meroni, D.; Falletta, E.; Pifferi, V.; Falciola, L.; Cappelletti, G.; Ardizzone, S. Emerging pollutant mixture mineralization by TiO₂ photocatalysts. The role of the water medium. *Photochem. Photobiol. Sci.* **2017**, *16*, 60–66. [[CrossRef](#)]
17. Detomaso, A.; Mascolo, G.; Lopez, A. Characterization of carbofuran photodegradation by-products by liquid chromatography/hybrid quadrupole time-of-flight mass spectrometry. *Rapid Commun. Mass Spectrom.* **2005**, *19*, 2193–2202. [[CrossRef](#)]
18. Malato, S. Removal of emerging contaminants in waste-water treatment: Removal by photo-catalytic processes. In *Emerging Contaminants from Industrial and Municipal Waste*; Springer: Berlin/Heidelberg, Germany, 2008; pp. 177–197.
19. Rimoldi, L.; Ambrosi, C.; Di Liberto, G.; Lo Presti, L.; Ceotto, M.; Oliva, C.; Meroni, D.; Cappelli, S.; Cappelletti, G.; Soliveri, G.; et al. Impregnation versus bulk synthesis: How the synthetic route affects the photocatalytic efficiency of Nb/Ta:N codoped TiO₂ nanomaterials. *J. Phys. Chem. C* **2015**, *119*, 24104–24115. [[CrossRef](#)]
20. Antonello, A.; Soliveri, G.; Meroni, D.; Cappelletti, G.; Ardizzone, S. Photocatalytic remediation of indoor pollution by transparent TiO₂ films. *Catal. Today* **2014**, *230*, 35–40. [[CrossRef](#)]
21. Luster, E.; Avisar, D.; Horovitz, I.; Lozzi, L.; Baker, M.A.; Grilli, R.; Mamane, H. N-doped TiO₂-coated ceramic membrane for carbamazepine degradation in different water qualities. *Nanomaterials* **2017**, *7*, 206. [[CrossRef](#)]
22. Ghosh, M.; Lohrasbi, M.; Chuang, S.S.C.; Jana, S.C. Mesoporous titanium dioxide nanofibers with a significantly enhanced photocatalytic activity. *ChemCatChem* **2016**, *8*, 2525–2535. [[CrossRef](#)]

23. Noorjahan, M.; Pratap Reddy, M.; Durga Kumari, V.; Lavédrine, B.; Boule, P.; Subrahmanyam, M. Photocatalytic degradation of H-acid over a novel TiO₂ thin film fixed bed reactor and in aqueous suspensions. *J. Photochem. Photobiol. A Chem.* **2003**, *156*, 179–187. [[CrossRef](#)]
24. Zertal, A.; Molnár-Gábor, D.; Malouki, M.A.; Sehili, T.; Boule, P. Photocatalytic transformation of 4-chloro-2-methylphenoxyacetic acid (MCPA) on several kinds of TiO₂. *Appl. Catal. B Environ.* **2004**, *49*, 83–89. [[CrossRef](#)]
25. Borges, M.; García, D.; Hernández, T.; Ruiz-Morales, J.; Esparza, P. Supported photocatalyst for removal of emerging contaminants from wastewater in a continuous packed-bed photoreactor configuration. *Catalysts* **2015**, *5*, 77–87. [[CrossRef](#)]
26. Murgolo, S.; Yargeau, V.; Gerbasi, R.; Visentin, F.; El Habra, N.; Ricco, G.; Lacchetti, I.; Carere, M.; Curri, M.L.; Mascolo, G. A new supported TiO₂ film deposited on stainless steel for the photocatalytic degradation of contaminants of emerging concern. *Chem. Eng. J.* **2017**, *318*, 103–111. [[CrossRef](#)]
27. Petronella, F.; Fanizza, E.; Mascolo, G.; Locaputo, V.; Bertinetti, L.; Martra, G.; Coluccia, S.; Agostiano, A.; Curri, M.L.; Comparelli, R. Photocatalytic activity of nanocomposite catalyst films based on nanocrystalline metal/semiconductors. *J. Phys. Chem. C* **2011**, *115*, 12033–12040. [[CrossRef](#)]
28. Daghrir, R.; Drogui, P.; Dimboukou-Mpira, A.; El Khakani, M.A. Photoelectrocatalytic degradation of carbamazepine using Ti/TiO₂ nanostructured electrodes deposited by means of a pulsed laser deposition process. *Chemosphere* **2013**, *93*, 2756–2766. [[CrossRef](#)] [[PubMed](#)]
29. Chen, X.; Mao, S.S. Titanium dioxide nanomaterials: Synthesis, properties, modifications, and applications. *Chem. Rev.* **2007**, *107*, 2891–2959. [[CrossRef](#)]
30. Robinson, B.W.; Tighe, C.J.; Gruar, R.I.; Mills, A.; Parkin, I.P.; Tabecki, A.K.; De Villiers Lovelock, H.L.; Darr, J.A. Suspension plasma sprayed coatings using dilute hydrothermally produced titania feedstocks for photocatalytic applications. *J. Mater. Chem. A* **2015**, *3*, 12680–12689. [[CrossRef](#)]
31. Chiarello, G.L.; Dozzi, M.V.; Selli, E. TiO₂-based materials for photocatalytic hydrogen production. *J. Energy Chem.* **2017**, *26*, 250–258. [[CrossRef](#)]
32. Chiarello, G.L.; Tealdi, C.; Mustarelli, P.; Selli, E. Fabrication of Pt/Ti/TiO₂ photoelectrodes by RF-magnetron sputtering for separate hydrogen and oxygen production. *Materials* **2016**, *9*, 279. [[CrossRef](#)] [[PubMed](#)]
33. Bestetti, M.; Franz, S.; Cuzzolin, M.; Arosio, P.; Cavallotti, P.L. Structure of nanotubular titanium oxide templates prepared by electrochemical anodization in H₂SO₄/HF solutions. *Thin Solid Films* **2007**, *505*, 5253–5258. [[CrossRef](#)]
34. Eskandarloo, H.; Hashempour, M.; Vincenzo, A.; Franz, S.; Badiei, A.; Behnajady, M.A.; Bestetti, M. High-temperature stable anatase-type TiO₂ nanotube arrays: A study of the structure-activity relationship. *Appl. Catal. B Environ.* **2016**, *185*, 119–132. [[CrossRef](#)]
35. Zlamal, M.; Macak, J.M.; Schmuki, P.; Krýsa, J. Electrochemically assisted photocatalysis on self-organized TiO₂ nanotubes. *Electrochem. Commun.* **2007**, *9*, 2822–2826. [[CrossRef](#)]
36. Yerokhin, A.L.; Nie, X.; Leyland, A.; Matthews, A.; Dowey, S.J. Plasma electrolysis for surface engineering. *Surf. Coat. Technol.* **1999**, *122*, 73–93. [[CrossRef](#)]
37. Teh, T.H.; Berkani, A.; Mato, S.; Skeldon, P.; Thompson, G.E.; Habazaki, H.; Shimizu, K. Initial stages of plasma electrolytic oxidation of titanium. *Corros. Sci.* **2003**, *45*, 2757–2768. [[CrossRef](#)]
38. Franz, S.; Perego, D.; Marchese, O.; Lucotti, A.; Bestetti, M. Photoactive TiO₂ coatings obtained by plasma electrolytic oxidation in refrigerated electrolytes. *Appl. Surf. Sci.* **2016**, *385*, 498–505. [[CrossRef](#)]
39. Franz, S.; Perego, D.; Marchese, O.; Bestetti, M. Photoelectrochemical advanced oxidation processes on nanostructured TiO₂ catalysts: Decolorization of a textile azo-dye. *J. Water Chem. Technol.* **2015**, *37*, 108–115. [[CrossRef](#)]
40. Murgolo, S.; Franz, S.; Arab, H.; Bestetti, M.; Falletta, E.; Mascolo, G. Degradation of emerging organic pollutants in wastewater effluents by electrochemical photocatalysis on nanostructured TiO₂ meshes. *Water Res.* **2019**, *164*, 114920. [[CrossRef](#)]
41. Chiarello, G.L.; Zuliani, A.; Ceresoli, D.; Martinazzo, R.; Selli, E. Exploiting the photonic crystal properties of TiO₂ nanotube arrays to enhance photocatalytic hydrogen production. *ACS Catal.* **2016**, *6*, 1345–1353. [[CrossRef](#)]
42. Pascual, J.; Camassel, J.; Mathieu, H. Fine structure in the intrinsic absorption edge of TiO₂. *Phys. Rev. B* **1978**, *18*, 5606–5614. [[CrossRef](#)]

43. Amtout, A.; Leonelli, R. Optical properties of rutile near its fundamental band gap. *Phys. Rev. B Condens. Matter.* **1995**, *15*, 6842–6851. [[CrossRef](#)] [[PubMed](#)]
44. Tang, H.; Lévy, F.; Berger, H.; Schmid, P.E. Urbach tail of anatase TiO₂. *Phys. Rev. B Condens. Matter.* **1995**, *15*, 7771–7774. [[CrossRef](#)] [[PubMed](#)]
45. Schollée, J.E.; Bourgin, M.; von Gunten, U.; McArdell, C.S.; Hollender, J. Non-target screening to trace ozonation transformation products in a wastewater treatment train including different post-treatments. *Water Res.* **2018**, *142*, 267–278. [[CrossRef](#)] [[PubMed](#)]
46. Schymanski, E.L.; Jeon, J.; Gulde, R.; Fenner, K.; Ruff, M.; Singer, H.P.; Hollender, J. Identifying small molecules via high resolution mass spectrometry: Communicating confidence. *Environ. Sci. Technol.* **2014**, *48*, 2097–2098. [[CrossRef](#)]
47. Liu, N.; Lei, Z.D.; Wang, T.; Wang, J.J.; Zhang, X.D.; Xu, G.; Tang, L. Radiolysis of carbamazepine aqueous solution using electron beam irradiation combining with hydrogen peroxide: Efficiency and mechanism. *Chem. Eng. J.* **2016**, *295*, 484–493. [[CrossRef](#)]
48. Ghasemian, S.; Nasuhoglu, D.; Omanovic, S.; Yargeau, V. Photoelectrocatalytic degradation of pharmaceutical carbamazepine using Sb-doped Sn80%-W20%-oxide electrodes. *Sep. Purif. Technol.* **2017**, *188*, 52–59. [[CrossRef](#)]
49. Martínez, C.; Canle, M.L.; Fernández, M.I.; Santaballa, J.A.; Faria, J. Kinetics and mechanism of aqueous degradation of carbamazepine by heterogeneous photocatalysis using nanocrystalline TiO₂, ZnO and multi-walled carbon nanotubes-anatase composites. *Appl. Catal. B Environ.* **2011**, *102*, 563–571. [[CrossRef](#)]
50. Bessa, V.S.; Moreira, I.S.; Murgolo, S.; Mascolo, G.; Castro, P.M.L. Carbamazepine is degraded by the bacterial strain *Labrys portucalensis* F11. *Sci. Total Environ.* **2019**, *690*, 739–747. [[CrossRef](#)]
51. Calza, P.; Medana, C.; Padovano, E.; Giancotti, V.; Baiocchi, C. Identification of the unknown transformation products derived from clarithromycin and carbamazepine using liquid chromatography/high-resolution mass spectrometry. *Rapid Commun. Mass Spectrom.* **2012**, *26*, 1687–1704. [[CrossRef](#)]
52. Rayaroth, M.P.; Prasanthkumar, K.P.; Kang, Y.-G.; Lee, C.-S.; Chang, Y.-S. Degradation of carbamazepine by singlet oxygen from sulfidized nanoscale zero-valent iron–citric acid system. *Chem. Eng. J.* **2020**, *382*, 122828. [[CrossRef](#)]
53. Mascolo, G.; Lopez, A.; Detomaso, A.; Lovecchio, G. Ion chromatography–electrospray mass spectrometry for the identification of low-molecular-weight organic acids during the 2,4-dichlorophenol degradation. *J. Chromatogr. A* **2005**, *1067*, 191–196. [[CrossRef](#)] [[PubMed](#)]
54. Spurr, R.A.; Myers, H. Quantitative analysis of anatase-rutile mixtures with an X-ray diffractometer. *Anal. Chem.* **1957**, *29*, 760–762. [[CrossRef](#)]
55. Trasatti, S.; Petrii, O.A. Real surface area measurements in electrochemistry. *J. Electroanal. Chem.* **1992**, *327*, 353–376. [[CrossRef](#)]
56. Khazri, H.; Hassine, S.B.; Ghorbel-Abid, I.; Kalfat, R.; Trabelsi-Ayadi, M. Presence of carbamazepine, naproxen, and ibuprofen in wastewater from northern Tunisia. *J. Environ. Forensics* **2019**, *20*, 121–128. [[CrossRef](#)]
57. Zhang, Y.; Geißen, S.-U.; Gal, C. Carbamazepine and diclofenac: Removal in wastewater treatment plants and occurrence in water bodies. *Chemosphere* **2008**, *73*, 1151–1161. [[CrossRef](#)] [[PubMed](#)]
58. Guijas, C.; Montenegro-Burke, J.R.; Domingo-Almenara, X.; Palermo, A.; Warth, B.; Hermann, G.; Koellensperger, G.; Huan, T.; Uritboonthai, W.; Aisporna, A.E.; et al. METLIN: A technology platform for identifying knowns and unknowns. *Anal. Chem.* **2018**, *90*, 3156–3164. [[CrossRef](#)]

